Current Research in Food Science 7 (2023) 100553

Contents lists available at ScienceDirect

Current Research in Food Science

journal homepage: www.sciencedirect.com/journal/current-research-in-food-science

Designing ultra-stable linseed oil-in-water Mickering emulsions using whey protein isolate cold-set microgels containing marjoram aqueous extract: Effect of pH and extract on rheological, physical, and chemical properties

Maryam Farahmand, Mohammad-Taghi Golmakani, Mehrdad Niakousari, Marjan Majdinasab, Seyed Mohammad Hashem Hosseini *

Department of Food Science and Technology, School of Agriculture, Shiraz University, Shiraz, Iran

ARTICLE INFO

Keywords:
Mickering emulsion
Salt-induced cold-set microgel
Marjoram extract
Linseed oil
Oxidative stability

ABSTRACT

In this study, whey protein isolate (WPI) cold-set microgels containing marjoram (*Origanum majorana*) aqueous extract (MAE) were prepared at different pHs (4.0, 5.0, and 6.0). After characterization, the microgel dispersion was used to stabilize linseed oil-in-water Mickering emulsions (MEs). The resultant MEs were then characterized in terms of physicochemical and rheological properties under the effect of pH and MAE addition. The morphology, particle size, zeta potential, and interfacial tension of microgels were affected by pH and MAE. XRD patterns showed the amorphous structure. Microgel-stabilized MEs did not reveal any significant sign of instability under gravity during 6 months of storage. All MEs had dominant elastic character. Despite the lowest zeta potential values, MEs prepared at pH 4 showed the highest physical stability against gravity but the lowest centrifugal stability against oiling off, which indicated that both viscous and elastic components are required for MEs stability. This sample had the highest apparent viscosity and the strongest viscoelastic properties. Rheological data were best fitted with Herschel-Bulkley and Power Law models. An increase in pH and presence of MAE improved the oxidative stability of MEs. The results of this study showed that WPI microgels are appropriate candidate for long-term stabilization of linseed oil-in-water MEs. The presence of MAE is useful in designing special emulsions in which the aqueous phase is partially replaced by the aqueous extract of medicinal plants.

1. Introduction

Emulsion stabilization using solid particles (also known as Pickering stabilization) is popular among many researchers due to low toxicity, cost effectiveness, appropriate taste and rheological properties, irreversible adsorption of particles to the interface and tailor-made droplet size, promoting an increase of physical stability. Micro or nanoparticles can promote an ultra-stability against destabilization mechanisms because of the high free energy of detachment from the interface (Jiang et al., 2020; Araiza-Calahorra et al., 2020).

Different particles based on animal and plant proteins, polysaccharides, protein–polysaccharide complexes, waxes, fat crystals, and flavonoids are common stabilizers in food-grade Pickering emulsions (Xia et al., 2021). Some researchers have explored the tuning of surface wettability of natural colloidal particles and designing micro or nanoparticles with improved interfacial properties. They also listed the potential advantages and drawbacks of Pickering particles as an alternative for chemical emulsifiers (Jiang et al., 2020).

Protein-based gel particles can be considered as a novel source of food-grade stabilizers. They are divided into microgels and nanogels. Pickering emulsions stabilized by semi-solid soft gel particles are defined as Mickering emulsions (MEs) (Jiang et al., 2020). Micro or nanogels can be fabricated by carrying out a top-down technique via applying controlled shear forces to previously prepared hydrogel networks. The resultant particulate system has good colloidal stability because of steric and electrostatic repulsions. The gel particles can also be produced from a protein dispersion subjected to cold-set gelation (known as bottom-up approach). This gelation process has two main steps: thermal denaturation, and salt- or acid-induced gelation (Lavoisier et al., 2019). After inducing the gelation process, the cold-set gel particles are fabricated under continuous stirring, whereas, the bulk gels are developed under quiescent conditions. Unlike heat-set gels, cold-set

* Corresponding author.
E-mail address: hhosseini@shirazu.ac.ir (S.M.H. Hosseini).

https://doi.org/10.1016/j.crfs.2023.100553
Received 4 June 2023; Received in revised form 9 July 2023; Accepted 20 July 2023
Available online 23 July 2023

counterparts are appropriate carriers for heat sensitive bioactive components.

Because of high nutritional value as well as appropriate techno-functional properties such as foaming, gelling, and emulsifying ability, whey proteins isolate (WPI) can be considered as an excellent source to fabricate gel particles. Various globular proteins in WPI including β-lactoglobulin, α-lactalbumin and bovine serum albumin are assembled into different types of aggregates depending on processing conditions such as pH, pressure, solvent quality, temperature, and ionic strength. The potential of WPI-based nanogels in the delivery of bioactive components has previously been explored (Schmitt et al., 2010).

Despite appropriate nutritional properties, bioactive lipids (particularly those rich in polyunsaturated fatty acids) suffer from high sensitivity to oxidative degradation and low solubility in water, which make their incorporation into aqueous foods and beverages challenging. Emulsion formation is the method of choice for incorporating lipids into aqueous systems. The oil droplets in O/W emulsions have increased specific surface area than bulk or non-emulsified lipids and thus are more vulnerable to the prooxidants in their vicinity (Rahiminezhad et al., 2020). Due to the large differences between the oxidation mechanisms in emulsified lipids and bulk lipids, appropriate preventive actions should be taken in emulsions mainly through tailoring the characteristics of interfacial film and utilization of efficient antioxidants.

Today, there is an increasing demand for natural antioxidants mainly due to the carcinogenic effects ascribed to synthetic ones (Shehata et al., 2021). Medicinal plants are considered as good sources of natural antioxidants. Marjoram (*Origanum majorana*) is a well-known herbal plant in Europe, northern Africa, and Asia. Previous researches have shown that the marjoram aqueous extract (MAE) is rich in phenolic compounds such as phenolic acids, flavonoids, and terpenoids. The phenolic acids include rosmarinic acid, carnosic acid, gallic acid, and ferulic acid. According to the numerous studies, MAE has also been known to be effective against irritated throat, rheumatism, headache, fever, insomnia, intestinal spasmodic, colds, flatulence, oral and digestive diseases, respiratory ailments, gastric disorders, neurological disorders, circulation system disorders, infusion against influenza and asthma, thyroid, cholesterol, hypoglycemia, and antiemetic (Bouyahya et al., 2021).

This study was performed in two steps. Firstly, changes in the physicochemical properties of WPI cold-set microgels, prepared by heat denaturation and salt-induced gelation, were evaluated under the effects of pH level and MAE concentration. Secondly, linseed oil-in-water (O/W) Mickering emulsions were stabilized by microgel particles and then investigated with regard to physical and chemical stability over storage at ambient temperature. The results of this study might help in designing special emulsions in which the aqueous phase is partially replaced by the aqueous extract of medicinal plants.

2. Materials and methods

2.1. Materials

Whey protein isolate (WPI) powder was supplied from Hilmar company (Hilmar, CA). Linseed oil (LO), extracted by cold press method, was purchased from a local store. Butylated hydroxytoluene (BHT) was supplied from Sigma-Aldrich (St. Louis, MO). Thiobarbituric acid (TBA), absolute ethanol, hydrochloric acid (HCl), trichloroacetic acid (TCA), sodium carbonate, and Folin–Ciocalteu reagent were supplied from Merck Co. (Darmstadt, Germany).

2.2. Marjoram extract preparation

Marjoram aqueous extract (MAE) was prepared using the method of Fontes-Candia et al. (2019) with some modifications. Marjoram (*Origanum majorana*) was bought from a local market and authenticated at Herbarium of Biology Department (Shiraz University, Iran). Dehydrated plant was milled and kept in sealed plastic bags at ambient temperature. The marjoram powder (20 g) was washed with deionized (DI) water and then mixed with boiling DI water (400 mL) for 5 min. The mixture was then cooled down to 35 °C and shaken for 24 h at 100 rpm, followed by filtration and centrifugation. The obtained aqueous extract was kept in 15 mL Falcon tubes at −80 °C until use.

2.3. Measurement of total phenolics of marjoram aqueous extract

Evaluation of total phenolic content was carried out according to the method described by Li et al. (2007) using gallic acid (0–30 mg/L) as a standard. 2 mL of MAE and 1 mL of Folin–Ciocalteu reagent (10%) were added to a test tube. After 4 min, 800 μL of sodium carbonate (75 g/L) was added. The absorbance at 765 nm was measured after incubation for 2 h. The amount of total phenolics was reported as gallic acid equivalent (GAE)/gram dry weight of marjoram.

2.4. Preparation of microgel dispersions

WPI (14 g) was dispersed in DI water (165 g) under magnetic stirring for 3 h at room temperature. The dispersion was kept at 4 °C for 8 h to achieve complete hydration. Sodium azide (0.03%, w/v) was used for microbial growth inhibition during the study. The dispersion was heated at 85 °C for 15 min to denature WPI molecules, followed by immediate cooling in an ice slurry. After that, it was homogenized for 2 min at 6000 rpm using Ultra-Turrax® (T18 digital, IKA-Werke GmbH & Co. KG, Germany) equipped with S18N-19G dispersing tool (stator diameter: 19 mm). $CaCl_2$ was added to the heated sample under constant stirring to reach 10 mM concentration. Then, DI water (119.3 g) and/or MAE (119.3 g) was added to the samples. The pH of protein dispersion was adjusted to 4, 5, or 6 using various HCl solutions. The dilution effect of acidification was considered negligible. To complete the fabrication of nanogel particles, 25 mL of microgel dispersions were poured into 50 mL Falcon tubes and stirred at room temperature for 24 h on a roller mixer (PiP, Tehran, Iran) at 60 rpm. The final concentrations of WPI and $CaCl_2$ in microgel dispersions were 4.7 wt% and 6 mM, respectively. The MAE content was 0 wt% or 40 wt%.

2.5. Analysis of microgel dispersion

2.5.1. Transmission electron microscopy (TEM)

TEM was carried out to study the morphology of microgel particles. One drop of each dispersion (already 5 times diluted with DI water at the same pH) was deposited onto a grid, negatively stained with uranyl acetate (2%), and air-dried. The morphological studies were carried out using TEM CM-10 (Philips Electronics, Eindhoven, Netherlands) at 80 kV. For each sample, five micrographs were captured and particle size distribution (expressed as number) was obtained by size measurement of at least 100 gel nanoparticles.

2.5.2. Size and zeta potential measurements

Volume-weighted mean hydrodynamic diameter, and magnitude of zeta potential of microgel particles were measured using photon correlation spectroscopy (DLS, SZ100, Horiba, Japan) at 25 °C. Microgel dispersions were 50 times diluted with DI water at the same pH. The refractive index of diluted samples was considered 1.33 (Sze et al., 2003). Volume-weighted mean diameter was reported as the central point. Span values (Eq. (1)) were considered as distribution width.

$$\text{Span} = (Dv_{0.9} - Dv_{0.1}) / Dv_{0.5} \quad (1)$$

Where, $Dv_{0.1}$, $Dv_{0.5}$ (median), and $Dv_{0.9}$ indicate particle sizes at which 10%, 50% and 90% of population lie below them, respectively.

2.5.3. X-ray diffraction (XRD)

After lyophilization of microgel dispersions using a freeze dryer

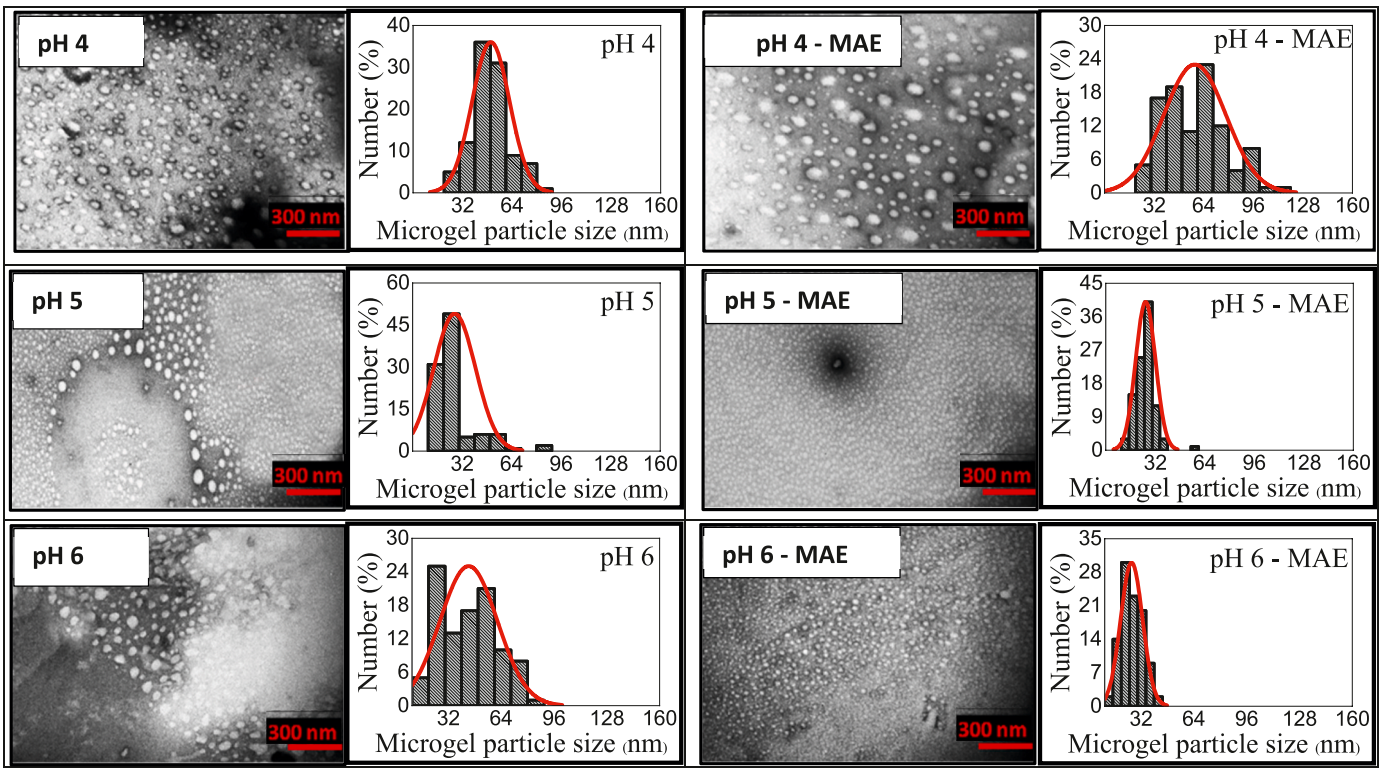

Fig. 1. TEM micrographs and respective number-weighted particle size distribution of WPI microgel particles prepared at different pH levels and in the absence or presence of 40 wt% marjoram aqueous extract (MAE).

(Vaco5, Zirbus Technology, Germany), the XRD pattern of microgel powders was evaluated using an X-ray diffractometer (Bruker, Germany) at 25 °C, 40 kV, and 40 mA. The spectra were recorded in 2θ range of 5–50° at 1 s step time.

2.5.4. Fourier transform infrared spectroscopy (FTIR)

Lyophilized microgel particles (1–2 mg) were blended with 200 mg of KBr, and then compressed to prepare the pellets. The spectra were recorded in range of 4000–400 cm^{-1} using Thermo Nicolet Avatar 370 spectrometer (Thermo Nicolet Corp., Madison, WI) at room temperature. In order to provide a deeper insight into the secondary structure of protein, derivatization was performed in the range of 1700–1600 cm^{-1} using OriginPro software (v2016 SR0, OriginLab Corporation, USA).

2.5.5. Interfacial tension

The ability of microgel particles to reduce interfacial tension (IFT) was determined using the pendant drop assay (DSA 100, KRÜSS GmbH, Hamburg, Germany). The image of a drop of WPI microgel dispersion (4.7 wt%), formed at the tip of a needle within bulk canola oil, was taken using a CCD camera and analyzed by Image J software (Image J 1.52p, National Institute of Health, USA). The IFT was determined by fitting the Laplace-Young equation (Soori et al., 2021).

2.6. Mickering emulsions (MEs) preparation

25 mL of linseed oil was added to 25 mL of different microgel dispersions followed by vigorous agitation. Homogenization was performed using an Ultra-Turrax® homogenizer (T18 digital, IKA-Werke GmbH & Co. KG, Germany) equipped with S18N-19G dispersing tool (stator diameter: 19 mm) at 9800 rpm for 5 min.

2.7. Characterization of Mickering emulsions

2.7.1. Gravitational stability

The emulsions were carefully poured into cylindrical glass tubes. The gravitational stability was monitored for 6 months. Creaming index (%) and oiling off (%) were calculated using Eq. (2) and Eq. (3), respectively.

$$\text{Creaming index } (\%) = (\text{Serum height} / \text{Total height}) \times 100 \quad (2)$$

$$\text{Oiling off } (\%) = (\text{Oil phase amount} / \text{Total amount}) \times 100 \quad (3)$$

2.7.2. Centrifugal stability

The emulsion samples (8 mL) were separately subjected to centrifugation at 2800*g* and/or 11,180 *g* for 10 min. The creaming index (%) and oiling off (%) were then calculated (section 2.7.1).

2.7.3. Colorimetric analysis

The color properties of MEs were evaluated using the method described by Gahruie et al. (2019). Photos were taken in a box equipped with a standard daylight source and analyzed by Adobe Photoshop® CS6 to determine *L*, *a*, and *b* values. Whiteness index (WI) and total color difference (ΔE) were calculated according to Eq. (4) and Eq. (5), respectively.

$$WI = 100 - \sqrt{(100 - L^*)^2 + a^{*2} + b^{*2}} \quad (4)$$

$$\Delta E = \sqrt{(L - L^*)^2 + (a - a^*)^2 + (b - b^*)^2} \quad (5)$$

where, L^*, a^*, and b^* are the color attributes of MEs just after preparation; *L*, *a*, and *b* are the color attributes after storing at ambient temperature for 6 months.

2.7.4. Optical light microscopy and size analysis

The emulsion droplets were observed immediately after preparation

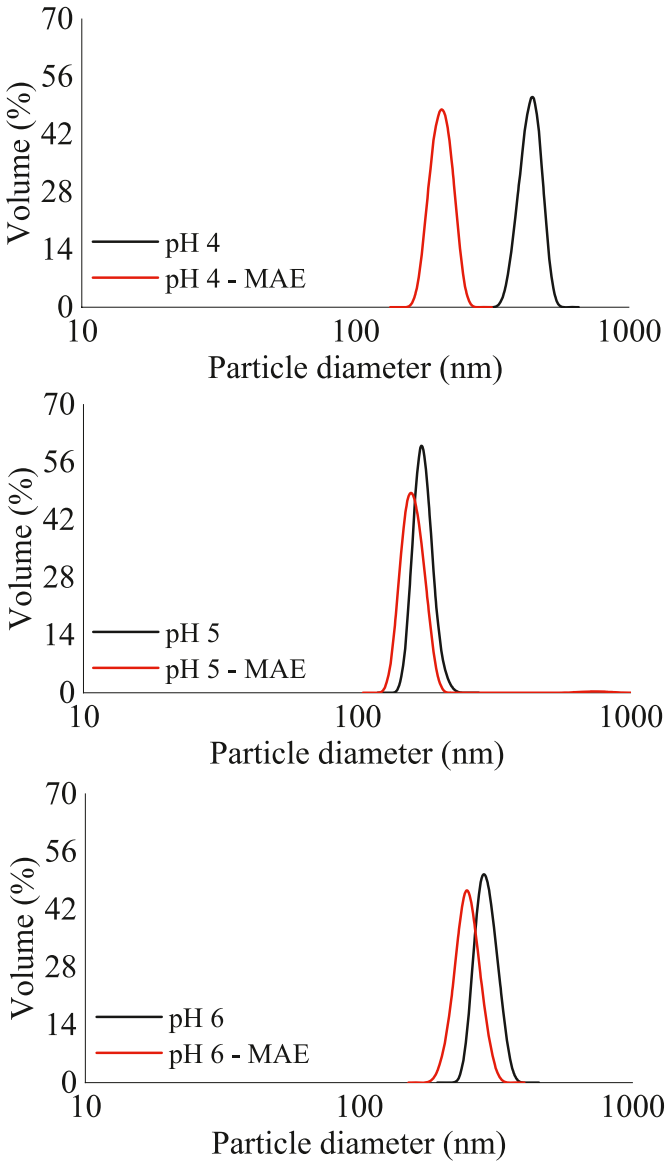

Fig. 2. Volume-weighted particle size distribution (obtained by DLS) of WPI microgel particles prepared at different pH levels and in the absence or presence of 40 wt% marjoram aqueous extract (MAE).

and after 6 months using an optical light microscope (Olympus CX40, Tokyo, Japan) equipped with a digital camera with an objective lens of 100 X. For each emulsion, ten micrographs were captured and then at least 100 droplets were photographed on graduated slide, followed by analyzing using Image J software. The droplet size distribution was then plotted using OriginPro software (Cochrane et al., 2017).

2.7.5. Zeta potential measurements

The zeta potential of ME droplets was measured using DLS SZ100 (Horiba, Japan). The samples were diluted 50 times using pre-adjusted DI water at the same pH of emulsions. The refractive index was considered as 1.33.

2.8. Rheological properties

2.8.1. Apparent viscosity

Changes in the apparent viscosity of MEs were investigated at 20 °C and shear rate range of 1–300 s^{-1} using MCR 302 rheometer (Anton Paar, Graz, Austria) (Gahruie et al., 2020). A cone and plate geometry

Table 1
Zeta-potential of microgels and respective Mickering emulsion oil droplets as well as volume-weighted mean diameter and Span values of microgels at different pH levels.

Microgels				Oil droplets
Sample	Zeta potential (mV)	Volume-weighted mean diameter (nm)	Span	Zeta potential (mV)
pH 4	−8.66 ± 0.58e	410.8 ± 23.4	0.186	−21.76 ± 0.45 d
pH 4 - MAE	−10.77 ± 0.35 d	194.4 ± 11.8	0.194	−16.14 ± 0.55e
pH 5	−24.96 ± 0.93 ab	164.0 ± 7.2	0.142	−47.80 ± 0.92 b
pH 5 - MAE	−26.70 ± 2.07a	188.1 ± 13.6	0.207	−46.37 ± 0.58 b
pH 6	−21.36 ± 0.23c	274.8 ± 16.4	0.195	−50.90 ± 1.87a
pH 6 - MAE	−24.43 ± 0.43 b	234.± 18.1	0.243	−42.73 ± 0.58c

Data are the average of three replicates ± standard deviation. In each column, different lowercase letters represent significant differences ($P < 0.05$). MAE indicates the presence of marjoram aqueous extract in the samples prepared at various pH levels.

(type CP25-1, cone diameter = 25 mm, gap size = 0.052 mm, and cone angle = 1°) was utilized. Before evaluation, the samples were temperature-equilibrated for 5 min. Shear stress vs. shear rate data was analyzed by usual rheological models namely Power Law, Herschel-Bulkley, Bingham, and Casson (Eqs. (6)–(9), respectively)

$$\tau = k\gamma^n \quad (6)$$

$$\tau = \tau_0 + k\gamma^n \quad (7)$$

$$\tau = \tau_0 + \mu\gamma \quad (8)$$

$$\tau = \tau_0^{0.5} + k\gamma^{0.5} \quad (9)$$

where the rheological parameters are shear rate (γ), shear stress (τ), yield stress (τ_0), consistency coefficient (k), flow behavior index (n), and Bingham viscosity (μ).

2.8.2. Viscoelasticity

Viscoelastic properties of MEs including storage (G') and loss (G'') moduli, loss factor (tan δ), and complex viscosity (η^*) were investigated at 20 °C using the same instrument (section 2.8.1). Firstly, linear viscoelastic region (LVR) was determined by strain sweep test at a range of 0.01%–100% and fixed frequency of 1 Hz. After that, frequency sweep test was performed within LVR (shear strain = 0.1%) and frequency range of 0.01–10 Hz.

2.8.3. Hysteresis loop

Hysteresis loop test was carried out to evaluate time-dependent flow behavior of MEs. The experiment was performed in a three-step cycle: the shear rate was increased from 1 to 300 s^{-1}, continued at 300 s^{-1} for 50 s, and finally decreased from 300 to 1 s^{-1}.

2.9. Lipid oxidation

The oxidation of linseed oil-in-water MEs and non-emulsified linseed oil was evaluated by measuring the secondary oxidation products at ambient temperature over time. 15 g TCA, 0.336 g TBA, 1.76 mL HCl (12 M), 82.8 g DI water, and 3 mL BHT solution (2 wt% in ethanol) were mixed and stirred for 15 min 2 g of the mixture and 2 g of the samples were poured into 15 mL tube and heated at 95 °C for 15 min. After rapid cooling to room temperature, centrifugation was done at 11,180 *g* for 10 min. The absorbance of pink aqueous phase was measured at 532 nm. The amounts of thiobarbituric acid reactive substances were determined

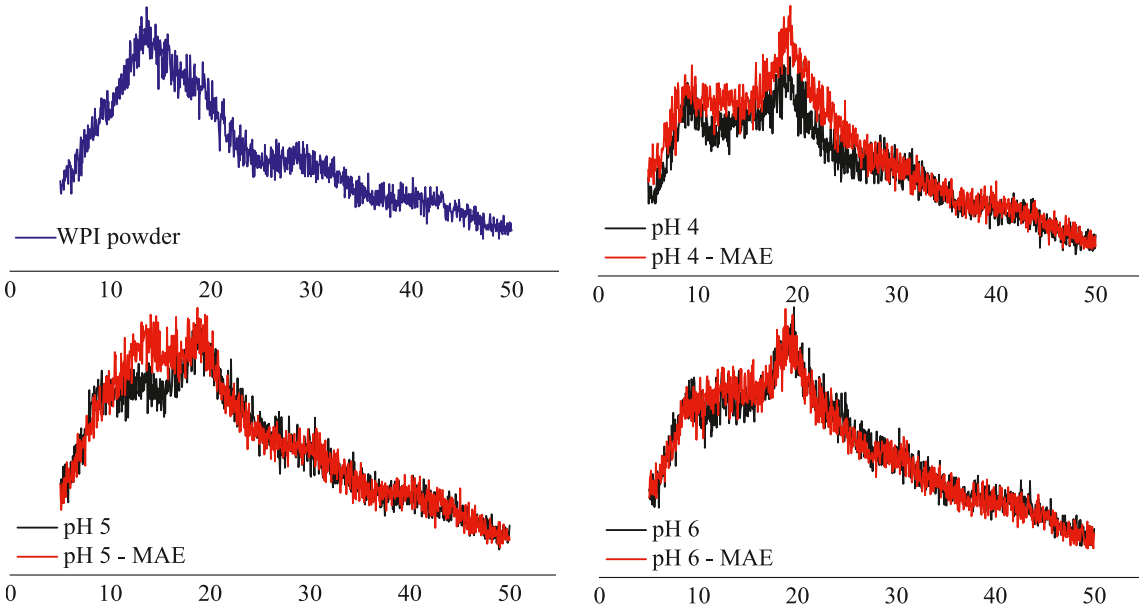

Fig. 3. X-ray diffraction pattern of WPI powder and respective WPI microgel particles prepared at different pH levels and in the absence or presence of 40 wt% marjoram aqueous extract (MAE).

Table 2
XRD peak assignment of WPI powder and respective WPI microgel particles prepared at different pH levels and in the absence or presence of 40 wt% marjoram aqueous extract (MAE).

	Whey powder	pH 4	pH 4 - MAE	pH 5	pH 5 - MAE	pH 6	pH 6 - MAE
2θ (°)	13.98	8.96, 19.05	8.94, 19.53	19.56	13.64, 19.07	11.82, 20.03	19.04

from the standard curve of malondialdehyde (mg MDA/Kg oil) (Sadeghian et al., 2023).

2.10. Statistical analysis

All tests were carried out in at least three times to report significant differences among the mean values. The statistical analysis software (SAS® software, ver. 9.1, SAS Institute Inc., NC, USA) was used for analyzing based on analysis of variance (ANOVA).

3. Results and discussions

3.1. Total phenolics of marjoram aqueous extract

Total phenolic content of MAE was 100 mg GAE/g dry weight of marjoram, which indicated a high level of phenolic content. Bakirtzi et al. (2016) studied the ultrasound-assisted extraction of some medicinal plants and reported that the marjoram extract had the highest amount (137.4 ± 9.8 mg GAE g^{-1} dw) of total polyphenols.

3.2. WPI microgel particles characteristics

3.2.1. Morphology

As shown in Fig. 1, microgel particles were oval or spherical; however, those prepared at pH 6 without MAE were of polygonal shape. The pH adjustment to various levels might cause denatured WPI molecules to undergo different aggregation modes, and formation of various nanogel particles. The higher negative charge on the protein surface at pH 6 might lead to the anisotropic growth of gel nanoparticles (Liu et al., 2021). The microgel particles prepared at pH 4 had the largest particle size among the other samples, which can be related to the self-aggregation and a complex interplay between the molecules close to the isoelectric pH of denatured WPI (Araiza Calahorra, 2020). Deformation of proteins' structure and subsequent aggregation depend on the equivalency of inter-/intra-molecular and attractive/repulsive forces among protein molecules, which are strongly influenced by the extrinsic conditions such as time-temperature profile, pH, and ionic strength (Liu et al., 2021). The microgel particles were individually dispersed indicating enough electrostatic repulsion among them to inhibit formation of the clustered structures (Araiza Calahorra, 2020). The number-weighted particle size distribution of gel particles (Fig. 1) revealed a range from 10 to 120 nm. The obtained geometric diameters were lower than the hydrodynamic diameters reported by DLS technique (Fig. 2), which can be related to the dehydration of microgels during sample preparation before TEM observation (Araiza Calahorra, 2020). Hydrodynamic diameter includes the hydrated layer around the nanoparticles. WPI nanoparticles with apparent diameter of 200–500 nm have been suggested as ideal candidates for stabilizing O/W emulsions (Wu et al., 2015). The addition of MAE, particularly at higher pH values, led to the formation of smaller nanogel particles. The polyphenolic compounds in MAE can interact with denatured WPI through van der Waals, electrostatic, hydrogen bonding, and hydrophobic interactions, and thus change the particle size via a shrinkage phenomenon (Baba et al., 2021).

3.2.2. Particle size and zeta potential

Fig. 2 shows the size distribution of different gel particles obtained by DLS. Moreover, the central points and distribution width are reported in Table 1. Generally, monomodal distributions (determined by Span values < 1) were observed in all samples. The results of DLS were in good agreement with those obtained by TEM. The largest and the smallest populations were observed at pH 4 and pH 5, respectively. Moreover, the addition of MAE shifted the particle size to smaller values. Several researchers reported that both pH variations and non-covalent complexation (i.e., by hydrogen bonding, van der Waal attractions, and hydrophobic interactions) of proteins and polyphenols can change

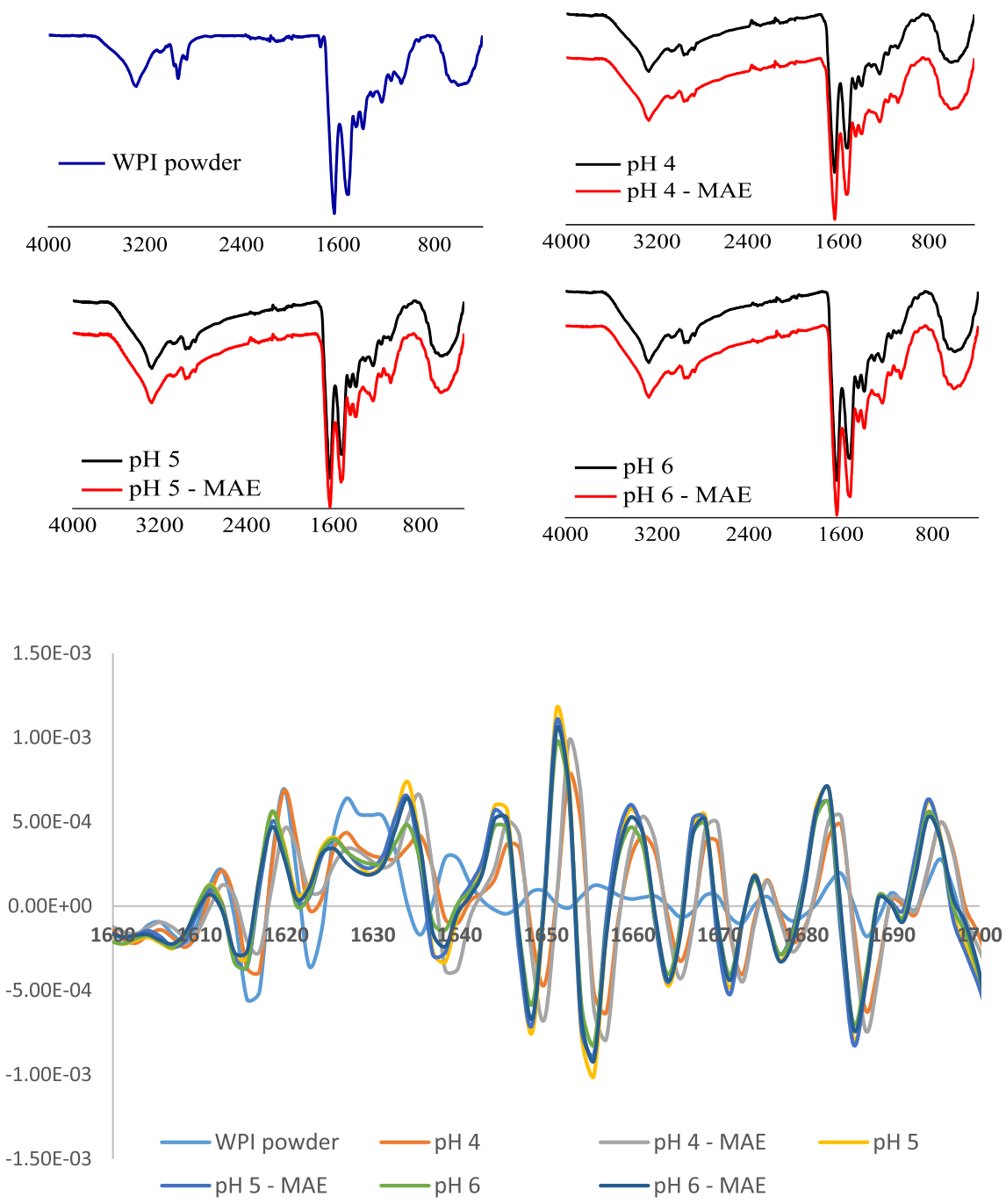

Fig. 4. Top panel: FTIR spectra of WPI powder and respective WPI microgel particles prepared at different pH levels and in the absence or presence of 40 wt% marjoram aqueous extract (MAE); Bottom panel: second derivative of the spectra at the wavenumber range of 1700–1600 cm^{-1}.

the quantity of proteins' secondary structures (Baba et al., 2021) and possibly led to a shrinkage of the microgel particles during preparation. Similar to our findings, Bahri et al. (2019) reported that the size of WPI-based particles increased by decreasing the pH during preparation. The size reduction might potentially increase the adsorption rate of microgel particles to the oil-water interface and increase the Mickering emulsion stability. However, an optimum size of microgel particles is required for the highest physical stability of emulsions. Small particles have too small free energy of detachment; thus, they are not able to strongly and irreversibly attach to the interface (Binks and Lumsdon, 2001).

Zeta potential values of gel particles are also reported in Table 1 pH reduction decreased the absolute values of zeta potential, which could be related to the protonation of carboxyl groups. The addition of MAE at 40 wt% significantly increased the zeta potential and subsequently the physical stability of microgel particles as a result of increased electrostatic repulsion. Polyphenols in MAE might change the secondary structure of denatured WPI and thus increase the exposure of negatively charged functions on protein microparticles. Proteins are positively charged at pH values lower than the isoelectric point (pI) and vice versa. Considering the pI value of WPI (4.7–5.2) and zeta-potential value of microgel particles at pH 4 (−8.66 mV), it can be concluded that heat denaturation and Ca^{2+}-induced gelation significantly changed the pI of microgel particles and shifted it towards lower values. This modification

Table 3
FT-IR peak assignment of WPI powder and respective WPI microgel particles prepared at different pH levels and in the absence or presence of 40 wt% marjoram aqueous extract (MAE).

Assignment	Wavenumber (cm $^{-1}$)						
	WPI powder	pH 4	pH 4 - MAE	pH 5	pH 5 - MAE	pH 6	pH 6 - MAE
N–H Stretching (amide A)	3272.76	3271.63	3272.11	3271.70	3271.91	3272.08	3271.59
NH stretching (amide B)	3078.30	3066.72	3078.74	3066.66	3078.78	3066.91	3078.66
C–H of methylene groups	2925.17	2960.24	2961.07	2956.99	2960.32	2960.33	2959.13
Symmetric stretching vibration of CH3	2854.63	2873.15	2873.61	2873.52	2873.69	2873.38	2873.22
Triple bands (C≡C and C≡N)	2324.09	2286.71	2324.77	2324.07	2278.70	2324.62	2324.07
	2163.32	2166.71	2106.45	2109.90	2166.00	2107.98	2110.78
C═O stretching, C–N stretching, N–H bending (amide I)	1629.44	1631.72	1631.66	1633.06	1633.04	1632.65	1633.17
N–H Bending, C–N Stretching (amide II)	1515.62	1518.23	1530.43	1518.87	1530.53	1518.68	1516.30
C═C bending	1449.37	1446.05	1444.79	1446.43	1444.82	1446.12	1445.31
C–N stretching, N–H bending, C═O stretching (amide III)	1235.33	1234.37	1233.56	1234.99	1236.30	1236.44	1235.75
				1310.28		1305.90	
C–N functions	1389.78	1391.06	1392.60	1392.56	1392.31	1392.98	1393.32
Stretching vibration C–C, C–O and bending vibration of C–O–H	1157.69	1162.56	1170.69	1159.35	1156.76	1159.24	1170.00
	1074.63	1075.84	1073.46	1075.79	1073.28	1077.08	1073.80
	928.52						
Bending vibration of N–H	600.22	597.11	602.34	606.71	609.43	604.30	609.71

Table 4
IFT values of WPI microgel particles prepared at different pH levels and in the absence or presence of 40 wt% marjoram aqueous extract (MAE).

Sample	pH 4	pH 4 - MAE	pH 5	pH 5 - MAE	pH 6	pH 6 - MAE
IFT (mN/m)	9.68 ± 0.57a	9.86 ± 0.11a	10.11 ± 0.92a	8.55 ± 0.36bc	9.24 ± 0.12 ab	7.94 ± 1.03c

Data are the average of three replicates ± standard deviation. Different lowercase letters are significantly different ($P < 0.05$).

might be resulted from the formation of intra- and inter-molecular disulfide bonds and rearrangement of charges which might lower the surface positive charges or redistribute surface amino acids and make them more negatively charged. Schmitt et al. (2007) reported a non-significant decrease in the zeta potential during the formation of β-lactoglobulin and WPI soluble aggregates that could result in more resistance to further aggregation in the presence of salts and with heat.

3.2.3. XRD

The crystalline state affects the solubility and the functionality of bioactive components (including protein microgel particles). It has been confirmed that in oral delivery systems, the amorphous state leads to a higher bioavailability than the crystalline state (Zhan et al., 2020). The XRD pattern of WPI powder and respective microgels are shown in Fig. 3. The quantitative data are also reported in Table 2. The pattern related to WPI powder had a broad peak at about 13.98°, which shows the amorphous nature of proteins (Zhan et al., 2020). Also, the microgel samples had broad and low-intensity peaks. These peaks and their shifts under the effect of pH and the presence of MAE could indirectly indicate that the polyphenolic compounds of MAE were entrapped within the protein gel matrix in an amorphous form (Solghi et al., 2020).

3.2.4. FTIR

The FTIR spectra and peak assignment of WPI powder and microgel particles are illustrated in Fig. 4 and Table 3, respectively. Slight shifts and changes in the amplitude were observed in the spectrum of each microgel system as compared to that of WPI powder. The observed peaks in the range of amide A (3272-3271 cm^{-1}) and amide B (3078-3066 cm^{-1}) were ascribed to hydrogen bonding and NH stretching. The results showed that the C–H of methylene groups (2925 cm^{-1}) shifted to higher wavenumbers (2959-2978 cm^{-1}) after heat denaturation and salt-induced formation of microgels. All samples showed the peaks in the range of 1633–1629 cm^{-1} (amide I) relating to the C═O stretching and the secondary structure of WPI. The peaks in the range of 1530–1515 cm^{-1} (amide II) were ascribed to the CO stretching and CN bending. All samples showed a peak within the range of 1449–1444 cm^{-1} indicating C═C bending. All samples showed peaks indicating C–N functions within the range of 1394–1389 cm^{-1}. The peaks in the range of 1200–800 cm^{-1} were attributed to the stretching vibration of C–C, C–O and bending vibration of C–O–H. The heating step changed the OH banding and NH stretching and shifted the peaks related to the amide B to the right. MAE addition also changed the OH banding and NH stretching, however, shifted the related peaks to the left. Chavoshpour-Natanzi and Sahihi (2019) similarly found out that binding WPI aggregates to quercetin can shift the peaks related to the OH-group and change the formation of hydrogen bonds. Adjusting pH value of microgels to pH 5 and pH 6 revealed two peaks (1310 and 1305 cm^{-1}, respectively) relating to C–N stretching, N–H bending, C═O stretching (amide III). Heating step and MAE addition at pH 5 could change C–H of methylene groups and shifted the related peaks. Heating step also changed the symmetric stretching vibration of CH3. MAE addition could change N–H bending and C–N stretching (amide II) at pH 4 and 5. Similar spectra have been reported in the previous studies: hydrogen bonding and NH stretching at 3294-3298 cm^{-1} (amide A), amide B at 3068-3071 cm^{-1}, C–H of methylene groups at 2925-2928 cm^{-1}, CO stretching in the range of 1700–1600 cm^{-1} (amide I), CN stretching and NH bending at 1247-1249 cm^{-1} (amide III), C═C bending at 1451-1454 cm^{-1}, C–N functions at 1393-1397 cm^{-1}, and stretching vibration of C–C, C–O and bending vibration of C–O–H at 800-1200 cm-1 (O'Loughlin et al., 2015). FTIR spectrum can give information about the secondary structure. Among different characteristic bands of protein, amide I band (1629 cm^{-1}) is the most sensitive region to the conformational changes of protein. Amide II band (1516 cm^{-1}) is also conformationally sensitive (Ferraro et al., 2015). The amide I band at around 1610-1640 cm^{-1}, 1640-1650 cm^{-1}, 1650-1660 cm^{-1}, and 1660-1695 cm^{-1} depict β-sheet, random coil, α-helix, and β-turns secondary structures, respectively. Accordingly, the main secondary structure of WPI (microgels) was β-sheet. Heating of WPI (during microgel formation) caused some structural changes so that the amide I bands shifted to higher wavenumbers (1631 cm^{-1} at pH 4 and 1632 cm^{-1} at pH 5 and pH 6, respectively). In addition, the intensity of amide I and amide II bands increased after heating that may be related to interactions between C–O groups and also C–N groups or the contribution of the C═O bonds to non-covalent polar interactions (Ferraro et al., 2015; Meng and Li, 2021). About the effect of pH, the secondary structure of the microgel sample at pH 4 showed slight differences with those at pH 5 and pH 6, which might be attributed to the structural changes of WPI at its isoelectric point (Table 1: close to pH 4). Changes

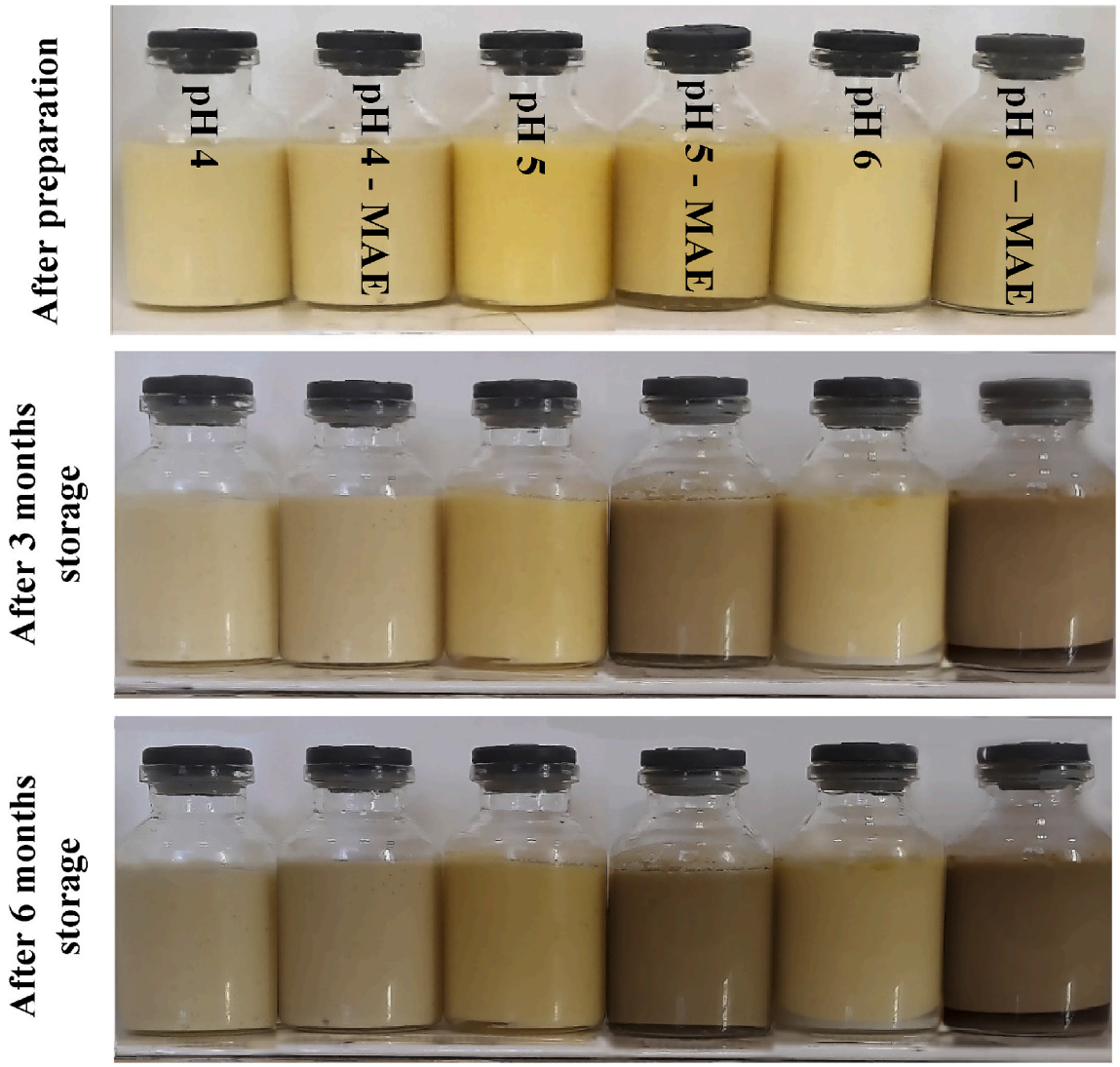

Fig. 5. Gravitational stability of microgel-stabilized O/W Mickering emulsions (MEs) over time; MEs were prepared at different pH levels and in the absence or presence of marjoram aqueous extract (MAE). The MAE content in final emulsions was 20 wt%.

Table 5
Gravitational and centrifugal stability of microgel-stabilized O/W Mickering emulsions.

Samples	Gravitational stability after 6 months		Centrifugal stability			
			2800 *g*		11,180 *g*	
	Creaming index (%)	Oiling off (%)	Creaming index (%)	Oiling off (%)	Creaming index (%)	Oiling off (%)
pH 4	100a[a]	ND	71.8 ± 1.0 b	ND	57.5 ± 5.3c	23.1 ± 1.9a
pH 4 - MAE	100a	ND	74.9 ± 0.1a	ND	61.9 ± 2.6 b	13.7 ± 1.3 b
pH 5	100a	ND	75.0 ± 3.5a	0.6 ± 0.1 b	63.8 ± 3.5 b	3.6 ± 0.1cd
pH 5 - MAE	96.9 ± 1.4a	ND	75.0 ± 0.1a	1.3 ± 0.1a	68.1 ± 0.9a	4.7 ± 0.3 d
pH 6	100a	ND	75.6 ± 1.0a	ND	71.9 ± 0.9a	1.1 ± 0.1e
pH 6 - MAE	90.95 ± 2.3 b	ND	75.5 ± 1.0a	ND	70.6 ± 0.8a	2.4 ± 0.2de

Data are the average of three replicates ± standard deviation. In each column, different lowercase letters are significantly different ($P < 0.05$). ND stands for non-Detected results.

[a] Higher values of creaming index indicate higher physical stability.

in the secondary structure are more obvious in the second derivative spectra of the amide I region of the samples (Fig. 4b). The general structure of microgels remained unchanged upon adding the extract and no new covalent bond was observed. This observation implies the occurrence of other types of interactions such as hydrogen bonding and hydrophobic interactions between the polyphenols in MAE and WPI. The slight changes in the intensity of amide I and II bands can be a proof for hydrophobic interactions (Ferraro et al., 2015). Similarly, Ferraro et al. (2015) and do Prado Silva et al. (2021) reported non-covalent interactions between WPI and phenolic compounds (Ferraro et al., 2015; do Prado Silva et al., 2021).

3.2.5. *Interfacial tension*

In emulsion systems, the emulsifiers can reduce the interfacial

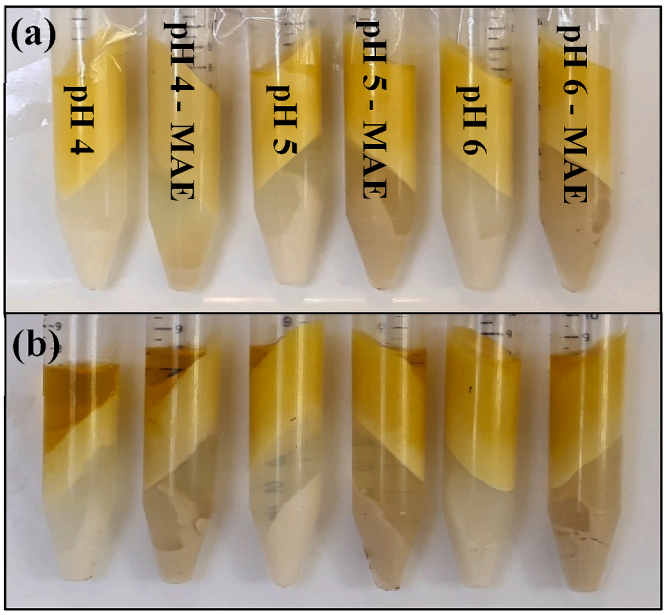

Fig. 6. Centrifugal stability of microgel-stabilized O/W Mickering emulsions (MEs) after centrifugation at (a) 2800 *g* and (b) 11,180 g for 10 min. MEs were prepared at different pH values and in the absence or presence of marjoram aqueous extract (MAE). The MAE content in final emulsions was 20 wt%.

tension (IFT), retard the coalescence, and facilitate the oil break up during the emulsification by decreasing the required energy (Gao et al., 2014). Individual protein molecules, protein aggregates and protein microgels possess a complex structure and can play role as the emulsifier. It has been previously hypothesized that the IFT and interfacial elasticity are the parameters that can be used to predict the stability of protein-based emulsions (Amine et al., 2014). The IFT results of microgel dispersions are reported in Table 4. The lowest values were measured in the samples containing MAE and adjusted to pH 6 and pH 5. Similarly, Amine et al. (2014) concluded that by increasing the proteins' absolute charge through increasing the pH to the values higher than pI, partial unfolding results in the better emulsification characteristics. At a same pH, the microgel samples containing MAE had lower IFT values than MAE-free dispersions. In addition to the effect of phenolic compounds on the protein's structure (e.g., more exposure of hydrophobic regions), free or unbound phenolic compounds might also be responsible for IFT reduction. Similarly, Cizauskaite et al. (2016) reported that the IFT between aqueous rosemary extract and olive oil was 30% lower than pure water-olive oil IFT.

3.3. Mickering emulsions characteristics

3.3.1. Gravitational and centrifugal stability

The results of gravitational stability of Mickering emulsions (MEs) over time are reported in Fig. 5 and Table 5. All freshly-prepared samples revealed an excellent physical stability. Slight aqueous phase separation was observed after 3 months only in the samples prepared at pH 5 and pH 6. Similarly, Boostani et al. (2020) reported that the protein-based Pickering emulsions prepared at lower pH (pH 4) were more stable than those prepared at higher pH values. The higher physical stability at lower pH (Table 5) might be attributed to a more balanced hydrophilic-hydrophobic character, proper wettability conditions of microgels at pH 4, as well as better viscoelastic characteristics of MEs. In addition to the above-mentioned explanation, the size of microgels can also be considered as an important factor in the adsorption kinetics to the interface. Free energy of detachment is the minimum required energy for the desorption of spherical particles (such as microgels) from the interface. It is calculated by Eq. 10 (Binks and Horozov, 2006).

$\Delta G_d = \pi r^2 \gamma_{ow} (1 - |\cos\theta|)^2$ (10) where, ΔG_d is the free energy of detachment; r is particle radius; γ_{ow} is the oil-water IFT; and θ is the contact angle of particles. From this equation, it can be concluded that the particle size (as r^2) has the dominant effect on ΔG_d. A higher ΔG_d indicates a higher physical stability. Microgels prepared at pH 4 had a larger particle size than those prepared at other pH levels (Table 1),

Table 6
Changes in the color parameters of microgel-stabilized O/W Mickering emulsions.

Color parameters	Storage time			
	Samples	After preparation	After 3 months	After 6 months
L	pH 4	70.02 ± 1.01Ba	63.10 ± 1.2Ab	60.34 ± 1.55Ac
	pH 4 - MAE	68.67 ± 0.57Ba	59.34 ± 1.15Bb	56.01 ± 1.12Bc
	pH 5	70.02 ± 1.12Ba	59.10 ± 1.2Bb	56.12 ± 1.01Bc
	pH 5 - MAE	65.65 ± .54Ca	44.35 ± 1.52Cb	40.01 ± 1.12Cc
	pH 6	73.03 ± 1.01Aa	59.02 ± 1.01Bb	56 ± 1.10Bc
	pH 6 - MAE	65.10 ± 1.2Ca	40.67 ± 1.53Db	34.65 ± 1.63Dc
a	pH 4	1.34 ± 0.47 cb	2.10 ± 1.3Da	2.01 ± 1.14Da
	pH 4 - MAE	3.01 ± 0.81Ba	2.67 ± 0.58Da	3.12 ± 1.06CDa
	pH 5	3.33 ± 0.47Bb	5.02 ± 1.14BCa	5.03 ± 1.05Ba
	pH 5 - MAE	5.02 ± 0.82Ac	6.0 2 ± 0.03Bb	7.34 ± 0.58Aa
	pH 6	1.35 ± 0.47Cc	3.65 ± .15CDb	4.01 ± 0.12BCa
	pH 6 - MAE	3.02 ± 0.81Bb	9.10 ± 1.2Aa	8.67 ± 0.58Aa
b	pH 4	17.10 ± 1.2Ea	23.1 ± 1.2DEa	23.20 ± 1.1Ea
	pH 4 - MAE	19.34 ± 0.58Db	23.67 ± .57Da	24.67 ± 1.15DEa
	pH 5	32.10 ± 1.1Ab	39.20 ± 1.1Aa	40.1 ± 1.3Aa
	pH 5 - MAE	26.67 ± 1.16Bb	29.20 ± 1.1Ca	29.34 ± 1.15Ca
	pH 6	21.20 ± 1.1Cb	33.30 ± 1.2Ba	33.67 ± 1.14Ba
	pH 6 - MAE	18.30 ± .57DEc	21.68 ± 1.15 Eb	26.20 ± 1.1Da

Samples	Total color difference (ΔE)		Whiteness index (WI)		
	After 3 months	After 6 months	After preparation	After 3 months	After 6 months
pH 4	9.25 ± 0.31Ea	2.66 ± 0.58Db	65.47 ± 0.35Aa	56.36 ± 0.27Ab	54.08 ± 0.61Ac
pH 4 - MAE	10.32 ± 0.46Ea	3.63 ± 0.43Cb	63.04 ± 0.34Ba	52.86 ± 0.68Bb	49.45 ± 0.43Bc
pH 5	13.18 ± 0.17Da	3.16 ± 0.00CDb	55.99 ± 0.56Da	43.17 ± 0.05Db	40.30 ± 0.02Dc
pH 5 - MAE	21.49 ± 1.50Ba	4.60 ± 0.44Bb	56.22 ± 0.74Da	36.32 ± 0.80 Eb	32.79 ± 0.45Ec
pH 6	18.60 ± 0.08Ca	3.16 ± 0.00CDb	65.74 ± 0.16Aa	47.22 ± 0.93Cb	44.43 ± .037Cc
pH 6 - MAE	25.31 ± 0.53Aa	7.43 ± 0.32Ab	60.36 ± 0.85Ca	36.18 ± 1.02 Eb	29.14 ± 0.98Fc

Color parameters: *L* (brightness or lightness); *a* (redness-greenness); and *b* (yellowness-blueness); MAE indicates the presence of marjoram aqueous extract in the samples prepared at various pH levels. For a same emulsion, different lowercase letters indicate significant differences ($P < 0.05$) over time. At a same storage time, different uppercase letters indicate significant differences ($P < 0.05$) among different emulsions.

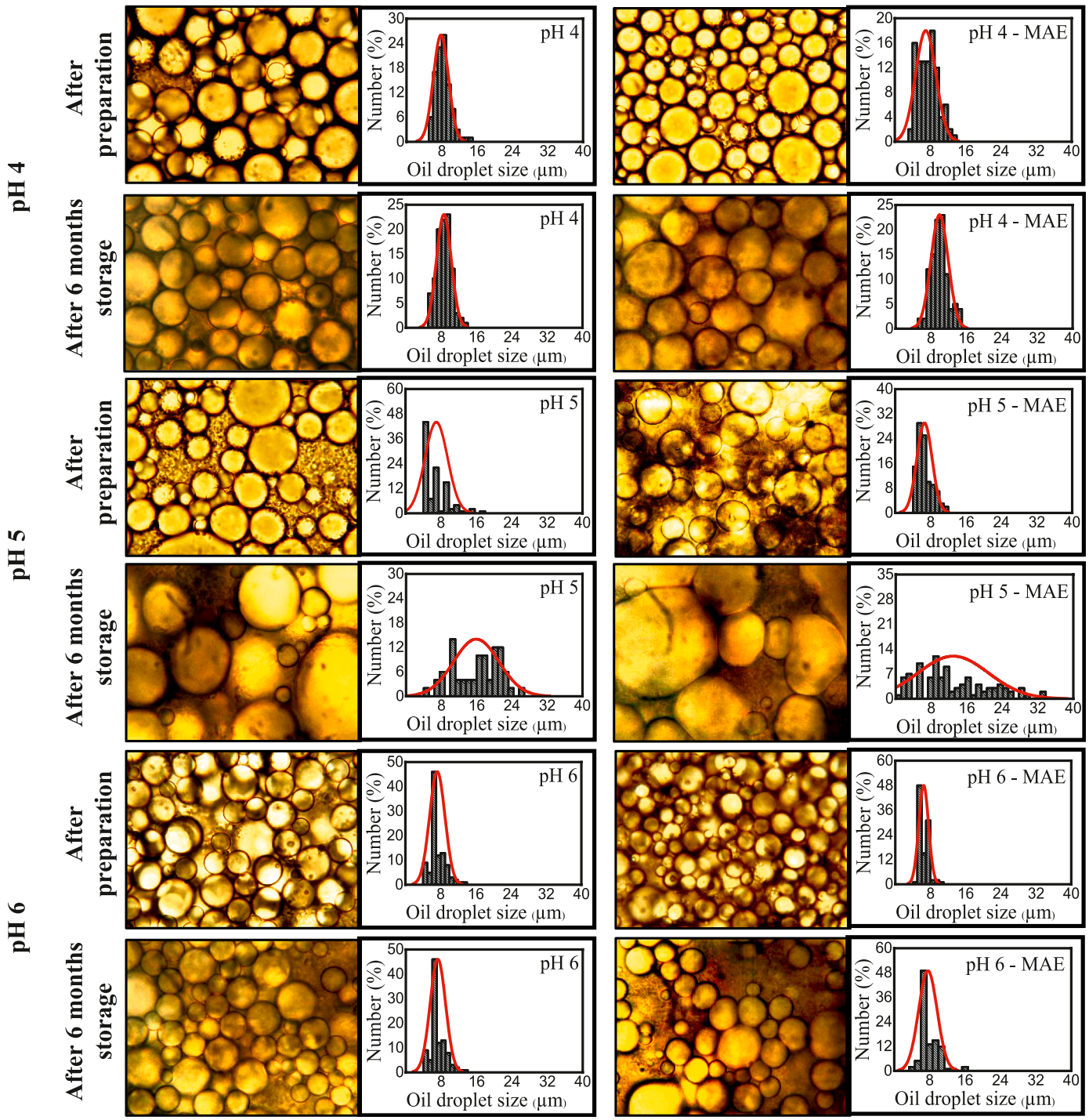

Fig. 7. Optical microscopy images and respective number-weighted droplet size distribution of Mickering emulsions prepared at different pH levels and in the absence or presence of 20 wt% marjoram aqueous extract (MAE).

which might lead to increase ΔG_d and thus the gravitational stability of respective ME. No evidence regarding the oiling off under the gravity was observed in the emulsions over time (Fig. 5). The turbidity of aqueous phase separated at pH 6 (indicating the presence of microgel particles) was higher than that separated at pH 5, which could be attributed to the higher hydrophilicity of microgel particles prepared at pH 6 (Fig. S1, supplementary data).

The results of centrifugal stability are shown in Fig. 6 and Table 5. The observed instabilities were dependent on the intensity of centrifugal force. Except for the samples prepared at pH 5, other MEs did not reveal any oiling off at 2800 *g*. All samples, particularly those prepared at pH 4, showed oiling off at 11,180 *g*. At pH 4, extensive oiling off against high centrifugal forces versus high physical stability under gravity might reflect the important effect of viscoelastic properties on the final stability of MEs. In other words, more elastic responses (Fig. 10) enhance the physical stability against the gravity, however, viscous characters are also required to some extent to prevent oiling off or the collapse of structure, particularly when the shear forces are above certain levels. The addition of MAE improved the stability of MEs against oiling off, particularly for those prepared at pH 4. Previous researches have shown that the polyphenol addition during particle preparation can result in size reduction and enhance the stability of protein-stabilized emulsions.

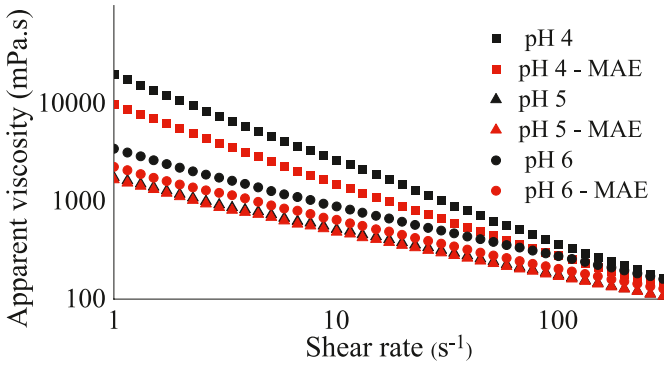

Fig. 8. Changes in the apparent viscosity of O/W Mickering emulsions (prepared at different pH levels and in the absence or presence of 20 wt% marjoram aqueous extract (MAE)) as a function of shear rate.

For instance, the catechin addition improved the stability of bran proteins-based emulsions and increased the proteins' surface hydrophobicity, which led to lower IFT and smaller oil droplets (Li et al., 2020; Yi et al., 2020).

3.3.2. Color parameters

The effects of pH and MAE on emulsions' color parameters are shown in Fig. 5 and Table 6. The decrease in lightness (L^*) during the first 3 months was noticeable. The L* continued to decrease until the end of storage but at a lower rate over the second 3 months. The addition of MAE significantly decreased the L^* of emulsions, which was attributed to the inherent color attributes of MAE ($L^*_{MAE} = 39.3 \pm 2.3$, $a^*_{MAE} = 34.3 \pm 1.2$, and $b^*_{MAE} = 24.7 \pm 3.2$). From a visual point of view, emulsion samples prepared at pH 4 were the most stable in terms of lightness. The samples containing MAE and prepared at pH 5 and pH 6 had the highest redness (a^*) value after 3 and 6 months. The highest amount of yellowness was measured in the sample prepared at pH 5 and remained maximum after 6 months of storage. Total color differences (ΔE) showed a significant decrease in the second 3-month period in comparison with the first 3-month period. Nearly all samples showed ΔE values more than 3 indicating that total differences in the color of emulsions were visible to naked eye during storage (Joukar et al., 2023). MAE-free sample at pH 4 and both samples at pH 5 had the highest and the lowest whiteness index (WI), respectively. Changes in the color parameters of emulsions were attributed to the both enzymatic and non-enzymatic interactions mediated by polyphenols (Jung et al., 2003) present in MAE as well as the oxidative degradation of unsaturated lipids and protein microgels.

3.3.3. Optical light microscopy and size analysis

Fig. 7 shows the optical light microscopy images of oil droplets stabilized by microgel particles at the beginning and after 6 months of storage. The number-weighted droplet size distribution is also reported in Fig. 7. The MEs prepared at pH 4 revealed more homogeneity, which resulted in better stability over time. After 6 months, the droplet size increased by coalescence and/or flocculation, particularly at pH 5, which led to the sign of aqueous phase separation. The emulsion prepared at pH 5 had the least viscosity among other samples, as well as a high heterogeneity in droplet size distribution. The addition of MAE to the aqueous phase reduced the average size of oil droplets. A further decrease was observed at higher pH values.

3.3.4. Zeta potential

Table 1 also reports the zeta potential values of microgel-stabilized oil droplets. A similar trend under the effect of pH and MAE addition was observed between the zeta potential values of oil droplets and individual WPI microgels (discussed earlier in section 3.2.2). However, the increase in the zeta potential absolute values of stabilized oil droplets could indicate the adsorption and packing of protein microgels at the O/W interface. Despite the lower zeta potential values of oil droplets at pH 4 (indicating lower electrostatic repulsion), the highest physical stability was observed at this pH (section 3.3.1). This was related to the kinetic energy barriers such as the high viscosity of continuous phase and viscoelastic properties of MEs.

3.3.5. Rheological properties

3.3.5.1. Flow behavior. As illustrated in Fig. 8, all MEs showed a pseudoplastic behavior. Similar behavior was reported by Xi et al. (2020) in the emulsions prepared with WPI-sugar conjugates at different pH values. During emulsification, a fraction of Pickering stabilizers might be shared between the oil droplets and led to some kind of flocculation. In emulsions, the shear thinning behavior is the result of the deflocculation of oil droplets under the applied shear (Boostani et al., 2020).

Table 7
Apparent viscosity and rheological analyses of O/W Mickering emulsions.

Sample		pH 4	pH 4 - MAE	pH 5	pH 5 - MAE	pH 6	pH 6 - MAE
η (mPa.s)		270.7 ± 38.7 ab	288.6 ± 24.2a	196.5 ± 15.0c	237.6 ± 32.4bc	62.6 ± 3.8 d	64.0 ± 1.8 d
Model	Constant						
Power Law	k (Pa.s^n)	9.54 ± 1.00a	3.93 ± 0.34 b	2.44 ± 0.34c	2.14 ± 0.28c	0.19 ± 0.02 d	0.17 ± 0.01 d
	n	0.10 ± 0.01e	0.34 ± 0.00 d	0.37 ± 0.01c	0.44 ± 0.01 b	0.70 ± 0.01a	0.73 ± 0.02a
	R^2 (%)	98.38 ± 0.00c	99.73 ± 0.00a	98.91 ± 0.02 b	99.95 ± 0.00a	99.96 ± 0.00a	99.97 ± 0.00a
	RMSE	0.40 ± 0.06 b	0.50 ± 0.03 b	0.80 ± 0.11a	0.22 ± 0.04c	0.09 ± 0.02 d	0.08 ± 0.01 d
Casson	k (Pa.s$^{0.5}$)	0.06 ± 0.01 b	0.18 ± 0.00 ab	0.17 ± 0.00 ab	0.44 ± 0.39a	0.16 ± 0.00 ab	0.17 ± 0.00 ab
	τ_0 (Pa)	10.46 ± 1.12a	5.40 ± 0.45 b	3.50 ± 0.44c	2.60 ± 1.35c	0.25 ± 0.04 d	0.22 ± 0.02 d
	R^2 (%)	93.54 ± 0.02 b	98.97 ± 0.00a	99.88 ± 0.00a	99.31 ± 0.00a	99.55 ± 0.00a	99.68 ± 0.00a
	RMSE	0.78 ± 0.07c	0.95 ± 0.06 b	0.25 ± 0.033 d	1.22 ± 0.14a	0.28 ± 0.01 d	0.25 ± 0.03 d
Bingham	μ (Pa.s)	0.02 ± 0.00 d	0.08 ± 0.00a	0.06 ± 0.00 b	0.08 ± 0.01a	0.03 ± 0.00cd	0.04 ± 0.00c
	τ_0 (Pa)	11.60 ± 1.36 d	7.67 ± 0.61a	5.18 ± 0.55 b	5.08 ± 0.68a	0.62 ± 0.08cd	0.58 ± 0.02c
	R^2 (%)	85.75 ± 0.03c	95.49 ± 0.00 b	98.10 ± 0.0 ab	96.24 ± 0.00 ab	98.68 ± 0.00a	99.00 ± 0.00a
	RMSE	1.15 ± 0.17 b	1.98 ± 0.13a	1.00 ± 0.01 b	1.85 ± 0.22a	0.47 ± 0.02c	0.43 ± 0.03c
Herschel-Bulkely	k (Pa.s^n)	6.70 ± 0.56a	2.02 ± 0.17 b	0.59 ± 0.00c	1.64 ± 0.15 b	0.15 ± 0.08c	0.17 ± 0.01c
	n	0.13 ± 0.02 d	0.44 ± 0.00c	0.61 ± 0.00 b	0.48 ± 0.01c	0.77 ± 0.12a	0.74 ± 0.03a
	τ_0 (Pa)	2.95 ± 1.23a	2.86 ± 0.24a	3.34 ± 0.55a	0.91 ± 0.25 b	0.31 ± 0.54 b	0.02 ± 0.03 b
	R^2 (%)	98.31 ± 0.00 b	99.97 ± 9.13a	99.98 ± 5.72a	99.98 ± 2.95a	99.73 ± 0.00a	99.96 ± 0.00a
	RMSE	0.40 ± 0.04a	0.14 ± 0.02 b	0.09 ± 0.01 b	0.09 ± 0.00 b	0.24 ± 0.27 ab	0.08 ± 0.01 b

Data are the average of three replicates ± standard deviation. In each row, different lowercase letters represent significant differences ($p < 0.05$). MAE indicates the presence of marjoram aqueous extract in the samples prepared at various pH levels. The MAE content in final emulsions was 20 wt%.

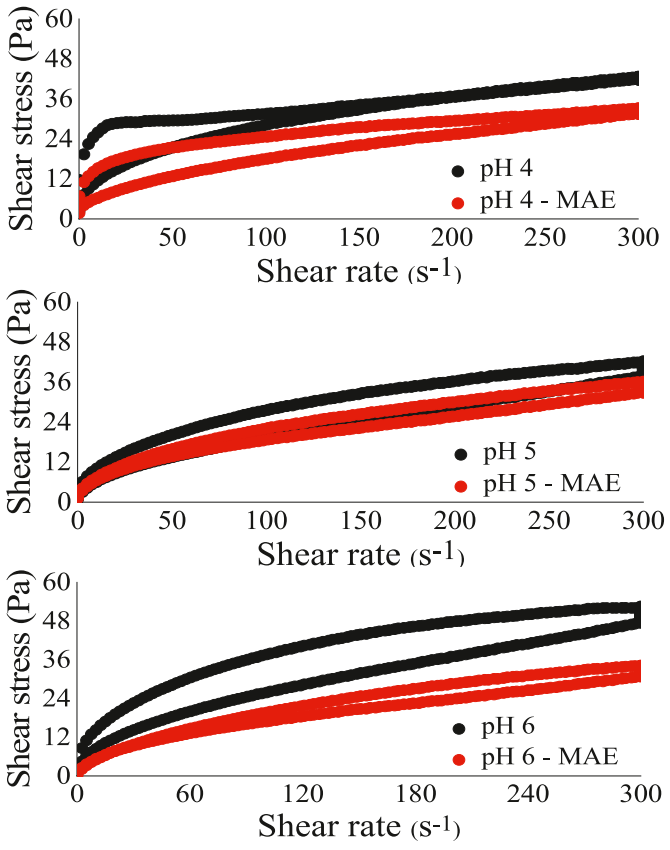

Fig. 9. Hysteresis loop test of O/W Mickering emulsions prepared at different pH levels and in the absence or presence of 20 wt% marjoram aqueous extract (MAE).

Table 7 reports the apparent viscosity of various emulsion samples at 50 s^{-1} and 20 °C. From Fig. 8 and Tables 7 and it can be concluded that pH reduction could significantly increase the apparent viscosity of final emulsions. The higher viscosity was attributed to the network entanglement or restricted molecular motions (Mahmood et al., 2018) mediated by the denatured protein microgels at pH values close to pI. Xi et al. (2020) similarly reported a higher viscosity of the emulsions stabilized by WPI-sugar conjugates at pH 4. The addition of MAE did not affect the flow behavior of MEs. The apparent viscosity was increased by MAE; however, it was not significant at a same pH value. Siebert et al. (1996) reported a pseudoplastic behavior in protein-polyphenol associations during the steady shear test. Table 7 also reports the constant parameters calculated for different rheological models. Taking into account R^2 and *RMSE* values, Herschel–Bulkley and Power Law models

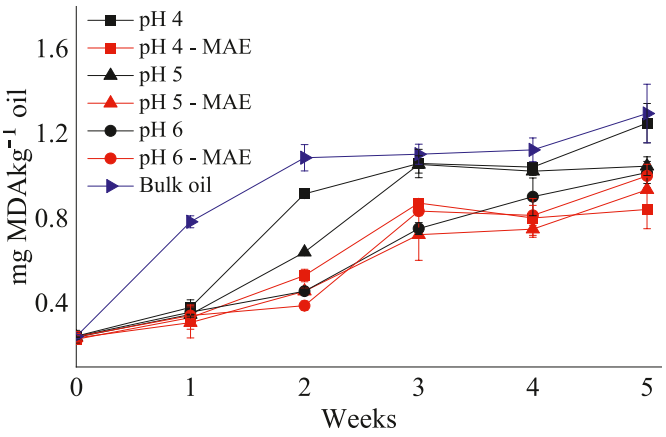

Fig. 11. Oxidative stability of bulk linseed oil and respective O/W Mickering emulsions determined by measuring TBARS values during storage for 5 weeks at room temperature; Mickering emulsions were prepared at different pH levels and in the absence or presence of 20 wt% marjoram aqueous extract (MAE).

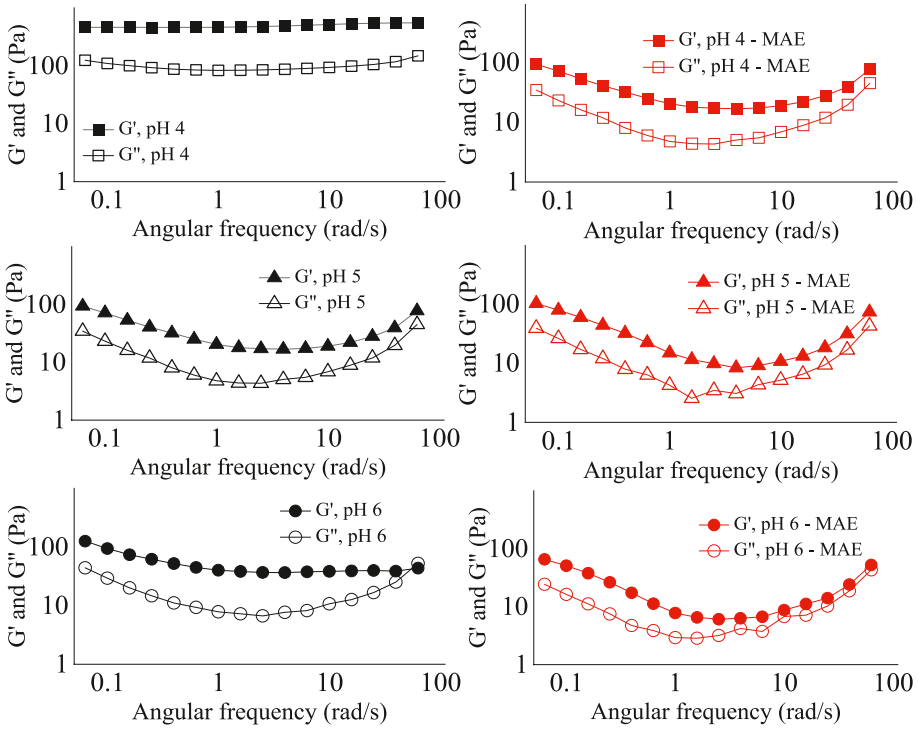

Fig. 10. Frequency sweep test of O/W Mickering emulsions prepared at different pH levels and in the absence or presence of 20 wt% marjoram aqueous extract (MAE).

were the best ones to describe the behavior of MEs. The indices of flow behavior (n) were <1 confirming the pseudoplasticity of samples. Samples prepared at pH 4 showed a stronger shear-thinning behavior (lower n values), which might be attributed to the higher interaction of microgel particles at the O/W interface and within the continuous phase. The higher pseudoplasticity might be responsible for the higher oiling off during centrifugation (section 3.3.1 and Fig. 6). MAE-free ME prepared at pH 4 showed the highest consistency coefficient (k).

3.3.5.2. Hysteresis loop. Time dependency and structural recovery are important characters in non-Newtonian materials. The results of hysteresis loop test are illustrated in Fig. 9. MEs prepared at pH 4 showed a thixotropic behavior or structural breakdown over time; while, those prepared at pH 5 and pH 6 revealed a structural build-up over time. The structural build-up over time might be attributed to the entrapment of aqueous phase within the flocculated oil droplets after subjecting to shear. The addition of MAE did not affect the time-dependent behavior of MEs prepared at different pH values. However, the hysteresis area between the upward and downward ramps (indicating the required energy to remove the effect of time in flow properties (Chandra and Shamasundar, 2015)) was significantly decreased.

3.3.5.3. Dynamic rheological properties. The results of amplitude (strain) sweep test are illustrated in Fig. S2. Regardless of pH and MAE addition, all MEs showed dominant elastic behavior or gel-like microstructure in LVE region. Similar results were reported by Sriprablom et al. (2019). The shear strain at which the crossover occurred ($G' = G''$) was affected by pH and MAE addition. The starting point of G' reduction by increasing the shear strain or the onset point of gel weakening was lower for MEs prepared at higher pH values. This result could be attributed to the less junction zones and the increase of required time to build up new entanglements for replacing those disrupted during the amplitude test (Alghooneh and Razavi, 2019). The results of frequency sweep tests are shown in Fig. 10. In all samples, dominant elastic behavior without any crossover was observed over the studied range of frequency. MEs prepared at pH 4 revealed significantly stronger viscoelastic properties than those prepared at pH 5 and pH 6, mainly due to a higher interaction among the stabilized oil droplets. At pH 4, G' and G'' showed almost no dependency on the frequency. However, a significant dependency was observed at pH 5 and pH 6, indicating a higher degree of structural breakdown and build-up of emulsions over time. The presence of MAE (particularly at pH 4) decreased the viscous and elastic moduli of MEs likely through the hydrophobic interactions between phenolic compounds and less charged microgel particles (Table 1) and thus affecting the wettability of microgels by the continuous phase. Changes in the complex viscosity and loss factor are reported in Fig. S3. The results of complex viscosity were in good agreement with those of steady shear test. Despite dominant elastic character, the loss factor values ($0.1 < \tan\delta < 1$) showed that the MEs were not real gels (Mandala et al., 2004) and applying high shear rates can temporarily disrupt the network connections (Rafe and Razavi, 2013).

3.3.6. Lipid oxidation

The droplet size and charge, effective surface area, interface layer thickness, presence of prooxidants (mainly transition metals) and antioxidants, and chemical nature of surfactant are the major factors influencing the oxidation of emulsions (Hu et al., 2003). Therefore, in emulsions, the oxidative stability is governed by the lipid phase, aqueous phase, and interfacial layer. In addition to providing physical stability, microgel particles should also be able to confer chemical stability to MEs against oxidation. Changes in TBARS values over time are shown in Fig. 11. Despite the large increase in the specific surface area of oil droplets as the result of emulsification, all MEs showed a higher chemical stability than the bulk linseed oil over time. This could be attributed to the packing of microgel particles at the interface and also to the antioxidant properties of MAE added to the aqueous phase. At a same pH value, particularly pH 4 and pH 5, the addition of MAE significantly retarded the oxidative instability of MEs. Almajano et al. (2007) showed that there was a synergistic effect between phenolic acids with proteins, which resulted in a better antioxidant activity in the emulsions than the proteins or phenolic acids separately. pH reduction significantly decreased the chemical stability of MEs. Decreasing the pH increases the solubility of transition metals (about 0.008 mg/g of WPI powder) and thus enhances their prooxidant activity. Moreover, pH reduction can increase the metal reducing capacity (i.e., $Fe^{3+} \rightarrow Fe^{2+}$) of phenolic acids (Friedman and Jürgens, 2000, Sugiarto et al., 2009) and thus increase the formation of stronger cations such as Fe^{2+}. In addition to pH-mediated changes in surface charge and its effect on oxidation, other factors such as the electrical charge of lipid substrate, surface absorption potential of free radicals, and different types of packing at the surface of oil droplets might be effective (Hu et al., 2003).

4. Conclusion

In this study, WPI cold set microgels were fabricated at different pH values and utilized in stabilizing linseed oil-in-water MEs. During preparation of microgel particles, a fraction of aqueous phase was replaced by MAE. Both pH and MAE addition affected the characteristics of microgel particles and resultant MEs. pH reduction improved the physical stability of MEs, however, decreased the oxidative stability. The addition of MAE improved both physical and chemical stability of MEs. The zeta potential of microgel-stabilized oil droplets was larger than that of microgel particles. The physical stability of MEs was mainly influenced by the rheological properties. The emulsion samples prepared at pH 4 had the least total color difference, while, those containing MAE and prepared at pH 5 and pH 6 had the highest total color differences after 3 and 6 months. WPI microgels containing MAE are appropriate Mickering stabilizers for the long-term physicochemical stability of linseed oil emulsions.

Credit author statement

M. Farahmand: Formal analysis, Investigation, Writing – original draft, **M.-T. Golmakani**: Supervision, Validation, Resources, Writing – review & editing, **M. Niakousari**: Validation, **M. Majdinasab:** Writing – original draft, **S.M.H. Hosseini**: Conceptualization, Resources, Funding acquisition, Supervision, Writing – review & editing.

Declaration of competing interest

The authors declare that they have no known competing financial interests or personal relationships that could have appeared to influence the work reported in this paper.

Data availability

Data will be made available on request.

Acknowledgment

The work was supported by Shiraz University (Grant Number 0GCB6M194065).

Appendix A. Supplementary data

Supplementary data to this article can be found online at https://doi.org/10.1016/j.crfs.2023.100553.

References

Alghooneh, A., Razavi, S.M., 2019. Transient and dynamic rheological properties of emerging hydrocolloids. Emerg. Nat. Hydrocolloids: Rheol. Funct. 101–134.

Almajano, M.P., Carbo, R., Delgado, M.E., Gordon, M.H., 2007. Effect of pH on the antimicrobial activity and oxidative stability of oil-in-water emulsions containing caffeic acid. J. Food Sci. 72 (5), C258–C263.

Amine, C., Dreher, J., Helgason, T., Tadros, T., 2014. Investigation of emulsifying properties and emulsion stability of plant and milk proteins using interfacial tension and interfacial elasticity. Food Hydrocolloids 39, 180–186.

Araiza Calahorra, A., 2020. Pickering Emulsion-Based Encapsulation Strategies for Delivery of Curcumin. Doctoral dissertation, University of Leeds.

Araiza-Calahorra, A., Wang, Y., Boesch, C., Zhao, Y., Sarkar, A., 2020. Pickering emulsions stabilized by colloidal gel particles complexed or conjugated with biopolymers to enhance bioaccessibility and cellular uptake of curcumin. Curr. Res. Nutr. Food Sci. 3, 178–188.

Baba, W.N., McClements, D.J., Maqsood, S., 2021. Whey protein–polyphenol conjugates and complexes: production, characterization, and applications. Food Chem. 365, 130455.

Bahri, A., Chevalier-Lucia, D., Marchesseau, S., Schmitt, C., Gergely, C., Martin, M., 2019. Effect of pH change on size and nanomechanical behavior of whey protein microgels. J. Colloid Interface Sci. 555, 558–568.

Bakirtzi, C., Triantafyllidou, K., Makris, D.P., 2016. Novel lactic acid-based natural deep eutectic solvents: efficiency in the ultrasound-assisted extraction of antioxidant polyphenols from common native Greek medicinal plants. J. Appl. Res. Med. Aromat. Plants. 3 (3), 120–127.

Binks, B.P., Horozov, T.S., 2006. Colloidal particles at liquid interfaces: an introduction. In: Binks, B.P., Horozov, T.S. (Eds.), Colloidal Particles at Liquid Interfaces. Cambridge University Press, New York, pp. 1–73.

Binks, B.P., Lumsdon, S.O., 2001. Pickering emulsions stabilized by monodisperse latex particles: effects of particle size. Langmuir 17 (15), 4540–4547.

Boostani, S., Hosseini, S.M.H., Golmakani, M.T., Marefati, A., Hadi, N.B.A., Rayner, M., 2020. The influence of emulsion parameters on physical stability and rheological properties of Pickering emulsions stabilized by hordein nanoparticles. Food Hydrocolloids 101, 105520.

Bouyahya, A., Chamkhi, I., Benali, T., Guaouguaou, F.E., Balahbib, A., El Omari, N., et al., 2021. Traditional use, phytochemistry, toxicology, and pharmacology of *Origanum majorana L.* J. Ethnopharmacol. 265, 113318.

Chandra, M.V., Shamasundar, B.A., 2015. Rheological properties of gelatin prepared from the swim bladders of freshwater fish Catla catla. Food Hydrocolloids 48, 47–54.

Chavoshpour-Natanzi, Z., Sahihi, M., 2019. Encapsulation of quercetin-loaded β-lactoglobulin for drug delivery using modified anti-solvent method. Food Hydrocolloids 96, 493–502.

Cizauskaite, U., Ivanauskas, L., Jakštas, V., Marksiene, R., Jonaitiene, L., Bernatoniene, J., 2016. *Rosmarinus officinalis L.* extract and some of its active ingredients as potential emulsion stabilizers: a new approach to the formation of multiple (W/O/W) emulsion. Pharmaceut. Dev. Technol. 21 (6), 716–724.

Cochrane, N.J., Lo, T.W., Adams, G.G., Schneider, P.M., 2017. Quantitative analysis of enamel on debonded orthodontic brackets. Am. J. Orthod. Dentofacial Orthop. 152 (3), 312–319.

do Prado Silva, J.T., Benetti, J.V.M., Alexandrino, T.T.D.B., Assis, O.B.G., de Ruiter, J., Schroën, K., Nicoletti, V.R., 2021. Whey protein isolate microgel properties tuned by crosslinking with organic acids to achieve stabilization of Pickering emulsions. Foods 10 (6), 1296.

Ferraro, V., Madureira, A.R., Sarmento, B., Gomes, A., Pintado, M.E., 2015. Study of the interactions between rosmarinic acid and bovine milk whey protein α-Lactalbumin, β-Lactoglobulin and Lactoferrin. Food Res. Int. 77, 450–459.

Fontes-Candia, C., Erboz, E., Martínez-Abad, A., López-Rubio, A., Martínez-Sanz, M., 2019. Superabsorbent food packaging bioactive cellulose-based aerogels from Arundo donax waste biomass. Food Hydrocolloids 96, 151–160.

Friedman, M., Jürgens, H.S., 2000. Effect of pH on the stability of plant phenolic compounds. J. Agric. Food Chem. 48 (6), 2101–2110.

Gahruie, H.H., Eskandari, M.H., Khalesi, M., Van der Meeren, P., Hosseini, S.M.H., 2020. Rheological and interfacial properties of basil seed gum modified with octenyl succinic anhydride. Food Hydrocolloids 101, 105489.

Gahruie, H.H., Eskandari, M.H., Van der Meeren, P., Hosseini, S.M.H., 2019. Study on hydrophobic modification of basil seed gum-based (BSG) films by octenyl succinate anhydride (OSA). Carbohydr. Polym. 219, 155–161.

Gao, Z.M., Yang, X.Q., Wu, N.N., Wang, L.J., Wang, J.M., Guo, J., Yin, S.W., 2014. Protein-based pickering emulsion and oil gel prepared by complexes of zein colloidal particles and stearate. J. Agric. Food Chem. 62 (12), 2672–2678.

Hu, M., McClements, D.J., Decker, E.A., 2003. Lipid oxidation in corn oil-in-water emulsions stabilized by casein, whey protein isolate, and soy protein isolate. J. Agric. Food Chem. 51 (6), 1696–1700.

Jiang, H., Sheng, Y., Ngai, T., 2020. Pickering emulsions: versatility of colloidal particles and recent applications. Curr. Opin. Colloid Interface Sci. 49, 1–15.

Joukar, F., Sadeghi, F., Naseri, M., Valizadeh, S., Esteghlal, S., Hosseini, S.M.H., 2023. Effects of active coatings based on soluble portion of zedo gum on physicochemical, microbial, and antioxidant enzymes characteristics of white shrimp. J. Food Meas. 17 (2), 1535–1547.

Jung, S., Ghoul, M., de Lamballerie-Anton, M., 2003. Influence of high pressure on the color and microbial quality of beef meat. LWT–Food Sci. Technol. 36 (6), 625–663.

Lavoisier, A., Vilgis, T.A., Aguilera, J.M., 2019. Effect of cysteine addition and heat treatment on the properties and microstructure of a calcium-induced whey protein cold-set gel. Curr. Res. Nutr. Food Sci. 1, 31–42.

Li, D., Zhao, Y., Wang, X., Tang, H., Wu, N., Wu, F., et al., 2020. Effects of (+)-catechin on a rice bran protein oil-in-water emulsion: droplet size, zeta-potential, emulsifying properties, and rheological behavior. Food Hydrocolloids 98, 105306.

Li, H.B., Cheng, K.W., Wong, C.C., Fan, K.W., Chen, F., Jiang, Y., 2007. Evaluation of antioxidant capacity and total phenolic content of different fractions of selected microalgae. Food Chem. 102 (3), 771–776.

Liu, X., Shen, L., Zhao, S., Zhang, H., 2021. Formation and emulsification properties of self-assembled potato protein microgel particles under different pH conditions. Int. J. Food Sci. Technol. 56 (6), 2864–2875.

Mahmood, K., Alamri, M.S., Abdellatif, M.A., Hussain, S., Qasem, A.A.A., 2018. Wheat flour and gum cordia composite system: pasting, rheology and texture studies. J. Food Sci. Technol. 38, 691–697.

Mandala, I.G., Savvas, T.P., Kostaropoulos, A.E., 2004. Xanthan and locust bean gum influence on the rheology and structure of a white model-sauce. J. Food Eng. 64 (3), 335–342.

Meng, Y., Li, C., 2021. Conformational changes and functional properties of whey protein isolate-polyphenol complexes formed by non-covalent interaction. Food Chem. 364, 129622.

O'Loughlin, I.B., Kelly, P.M., Murray, B.A., FitzGerald, R.J., Brodkorb, A., 2015. Concentrated whey protein ingredients: a fourier transformed infrared spectroscopy investigation of thermally induced denaturation. Int. J. Dairy Technol. 68 (3), 349–356.

Rafe, A., Razavi, S.M., 2013. Dynamic viscoelastic study on the gelation of basil seed gum. Int. J. Food Sci. 48 (3), 556–563.

Rahiminezhad, Z., Gahruie, H.H., Esteghlal, S., Mesbahi, G.R., Golmakani, M.T., Hosseini, S.M.H., 2020. Oxidative stability of linseed oil nano-emulsions filled in calcium alginate hydrogels. LWT–Food Sci. Technol. 127, 109392.

Sadeghian, S.F., Majdinasab, M., Nejadmansouri, M., Hosseini, S.M.H., 2023. Effects of natural antioxidants and high-energy fabrication methods on physical properties and oxidative stability of flaxseed oil-in-water nanoemulsions. Ultrason. Sonochem. 92, 106277.

Schmitt, C., Bovay, C., Rouvet, M., Shojaei-Rami, S., Kolodziejczyk, E., 2007. Whey protein soluble aggregates from heating with NaCl: physicochemical, interfacial, and foaming properties. Langmuir 23 (8), 4155–4166.

Schmitt, C., Moitzi, C., Bovay, C., Rouvet, M., Bovetto, L., Donato, L., Leser, M.E., Schurtenberger, P., Stradner, A., 2010. Internal structure and colloidal behaviour of covalent whey protein microgels obtained by heat treatment. Soft Matter 6 (19), 4876–4884.

Shehata, M.G., Awad, T.S., Asker, D., El Sohaimy, S.A., Abd El-Aziz, N.M., Youssef, M.M., 2021. Antioxidant and antimicrobial activities and UPLC-ESI-MS/MS polyphenolic profile of sweet orange peel extracts. Curr. Res. Nutr. Food Sci. 4, 326–335.

Siebert, K.J., Troukhanova, N.V., Lynn, P.Y., 1996. Nature of polyphenol– protein interactions. J. Agric. Food Chem. 44 (1), 80–85.

Solghi, S., Emam-Djomeh, Z., Fathi, M., Farahani, F., 2020. The encapsulation of curcumin by whey protein: assessment of the stability and bioactivity. J. Food Process. Eng. 43 (6), e13403.

Soori, T., Rassoulinejad-Mousavi, S.M., Zhang, L., Rokoni, A., Sun, Y., 2021. A machine learning approach for estimating surface tension based on pendant drop images. Fluid Phase Equil. 538, 113012.

Sriprablom, J., Luangpituksa, P., Wongkongkatep, J., Pongtharangkul, T., Suphantharika, M., 2019. Influence of pH and ionic strength on the physical and rheological properties and stability of whey protein stabilized o/w emulsions containing xanthan gum. J. Food Eng. 242, 141–152.

Sugiarto, M., Ye, A., Singh, H., 2009. Characterisation of binding of iron to sodium caseinate and whey protein isolate. Food Chem. 114 (3), 1007–1013.

Sze, A., Erickson, D., Ren, L., Li, D., 2003. Zeta-potential measurement using the Smoluchowski equation and the slope of the current–time relationship in electroosmotic flow. J. Colloid Interface Sci. 261 (2), 402–410.

Wu, J., Shi, M., Li, W., Zhao, L., Wang, Z., Yan, X., et al., 2015. Pickering emulsions stabilized by whey protein nanoparticles prepared by thermal cross-linking. Colloids Surf. B Biointerfaces 127, 96–104.

Xi, C., Kang, N., Zhao, C., Liu, Y., Sun, Z., Zhang, T., 2020. Effects of pH and different sugars on the structures and emulsification properties of whey protein isolate-sugar conjugates. Food Biosci. 33, 100507.

Xia, T., Xue, C., Wei, Z., 2021. Physicochemical characteristics, applications and research trends of edible Pickering emulsions. Trends Food Sci. Technol. 107, 1–15.

Yi, J., Qiu, M., Liu, N., Tian, L., Zhu, X., Decker, E.A., McClements, D.J., 2020. Inhibition of lipid and protein oxidation in whey-protein-stabilized emulsions using a natural antioxidant: black rice anthocyanins. J. Agric. Food Chem. 68 (37), 10149–10156.

Zhan, X., Dai, L., Zhang, L., Gao, Y., 2020. Entrapment of curcumin in whey protein isolate and zein composite nanoparticles using pH-driven method. Food Hydrocolloids 106, 105839.